Automated electrocorticographic electrode localization on individually rendered brain surfaces

Dora Hermes[a], Kai J. Miller[b], Herke Jan Noordmans[c], Mariska J. Vansteensel[a], Nick F. Ramsey[a,*]

[a] *Rudolf Magnus Institute of Neuroscience, University Medical Center Utrecht, Department of Neurology and Neurosurgery,*
Section Brainfunction and Plasticity, Utrecht, The Netherlands
[b] *Neurobiology and Behavior, University of Washington, Seattle, WA, United States*
[c] *Department of Medical Technology and Clinical Physics, University Medical Center Utrecht, Utrecht, The Netherlands*

ARTICLE INFO

ABSTRACT

Brain surface electrocorticographic (ECoG) recordings can investigate human brain electrophysiology at the cortical surface with exceptionally high signal to noise ratio and spatio-temporal resolution. To be able to use the high spatial resolution of ECoG for accurate brain function mapping and neurophysiology studies, the exact location of the ECoG electrodes on the brain surface should be known. Several issues complicate robust localization: surgical photographs of the electrode array made after implantation are often incomplete because the grids may be moved underneath the skull, beyond the exposed area. Computed tomography (CT) scans made after implantation will clearly localize electrodes, but the effects of surgical intervention may cause the exposed brain to move away from the skull and assume an unpredictable shape (the so-called brain shift). First, we present a method based on a preoperative magnetic resonance imaging (MRI) coregistered with a post-implantation CT scan to localize the electrodes and that automatically corrects for the brain shift by projecting the electrodes to the surface of the cortex. The calculated electrode positions are visualized on the individual subjects brain surface rendering. Second, the method was validated by comparison with surgical photographs, finding a median difference between photographic and calculated electrode centers-of-mass of only 2.6 mm, across 6 subjects. Third, to illustrate its utility we demonstrate how functional MRI and ECoG findings in the same subject may be directly compared in a simple motor movement experiment even when electrodes are not visible in the craniotomy.

© 2009 Elsevier B.V. All rights reserved.

1. Introduction

One of the latest additions to the cognitive neuroscience toolbox is electrocorticography (ECoG), where detailed information about the regional and functional organization of the brain is obtained from patients who are implanted with cortical electrodes for diagnostic purposes. Human ECoG is unique in the detail of electrical signal properties (e.g. spatial (Cooper et al., 1965) and temporal (Miller et al., 2009) resolution), and is growingly applied to cognitive paradigms in the service of cognitive neuroscience. Although patients, typically suffering from epilepsy, exhibit abnormal activity in some brain regions, most of the electrodes cover healthy brain tissue, allowing for extrapolation of findings in cognitive experiments to the normal population.

ECoG recordings measure the electrical potential from the brain surface, using exposed metal electrodes. ECoG recordings are used to functionally identify different brain areas such as motor (Crone et al., 1998a,b; Miller et al., 2007a; Pfurtscheller et al., 2003), language (Crone et al., 2001a,b; Sinai et al., 2005), auditory (Edwards et al., 2005), and visual cortex (Yoshor et al., 2007), or, for example, to study spontaneous neuronal activity (Nir et al., 2008) and neurophysiology (Canolty et al., 2006). The analyses of ECoG electrode signals are done on individual patients and above all are highly specific to the brain tissue from which signal is sampled (Ball et al., 2009). Electrodes are typically 2.3 mm in diameter and measure virtually no signal from immediately adjacent neural tissue. A major problem faced in ECoG research is to identify exactly where these electrodes are located. Rough estimations are, given the size of electrodes, insufficient for application of ECoG to neuroscientific questions regarding the regional and functional organization of the brain.

Several issues complicate accurate localization of these electrodes. First, matching photographs made of the grid after implantation to an MRI scan (Wellmer et al., 2002), are not sufficient, since neurosurgeons try to minimize the size of the cran-

* Corresponding author at: Department of Neurology and Neurosurgery, Heidelberglaan 100, G03.124, 3584 CX, Utrecht, The Netherlands. Tel.: +31 88 7556863; fax: +31 30 2542100.

E-mail address: n.ramsey@umcutrecht.nl (N.F. Ramsey).

iotomy and will usually slide electrodes under the skull, away from the exposed area. Second, computed tomography (CT) scans, made after implantation, can localize electrode positions (Noordmans et al., 2001), but the shape of the brain surface is generally changed by the surgical procedure. Leakage of CSF after opening of the dura, the thickness of the implanted material, and the general reaction to surgical intervention, may all cause the exposed brain to move away from the skull and assume an unpredictable shape. This brain shift may cause a significant mismatch that can be more than 1 cm between the CT scan and a magnetic resonance image (MRI) scan obtained preoperatively (Dalal et al., 2008; Hill et al., 2000). Third, post-implantation structural MRI scans would offer a solution to this problem (Schulze-Bonhage et al., 2002; Studholme et al., 2001), but the clinical safety guidelines of many institutions prohibit post-implant MRI scans for the risk of electrode induction heating (Bhavaraju et al., 2002).

Apart from the few studies using post-implant MRI scans, all papers on ECoG that we are aware of use either a match of MRI rendering to photos, hence ignoring the electrodes positioned under the skull and out of view of a camera, or ignore the shift after matching CT to MRI. Several studies projected electrode locations to a standardized brain in Talairach coordinates using a method based upon X-rays (Miller et al., 2007b), but this method suffers from the fact that identified electrode locations cannot be linked to subject-specific gyral anatomy, which can vary greatly from person to person. Dalal et al. (2008) approached the problem using operative photos to visually localize the ECoG electrodes on a reconstructed cortex from a preoperative MRI, and combined this with X-rays to include electrodes not visible in the craniotomy. Their manual registration procedure, however, takes quite long, even with experience, and it has not been established whether their method is reproducible across experimenters, or whether it might also work to localize subtemporal or interhemispheric electrodes (where no part of the array is revealed by the craniotomy, making extrapolation less reliable).

Here we present a new method that uses a preoperative MRI coregistered with a post-implantation CT scan to localize the electrodes, and then automatically corrects for the brain shift by projecting the electrodes to the surface of the cortex. It consists of a MATLAB (The Mathworks, Inc., Natick, MA, USA) based package used in combination with SPM5 software (http://www.fil.ion.ucl.ac.uk/spm/). To validate the accuracy of the projection, the auto-registered electrode locations are compared with operative photographs in six patients. For one additional patient we illustrate the usefulness of this method, by showing that electrodes outside the craniotomy can now be included in, for instance, investigation of the relationship between fMRI activation and ECoG.

2. Materials and methods

2.1. Patients

Seven patients were implanted with platinum electrodes (AdTech, Racine, WI, USA) for epilepsy monitoring. Electrodes had a diameter of 2.3 mm exposed (4.0 mm overall) and an inter-electrode distance of 1 cm center-to-center. All patients gave written informed consent, and the study was approved by the ethical committee of the University Medical Centre Utrecht, in accordance with the Declaration of Helsinki 2004.

2.2. Technique

Before implantation, structural MRI scans were made on a 1.5 T (patients 2, 3, 6 and 7) or 3 T (patients 1 and 4–5) scanner (Philips Achieva, Best, The Netherlands). Voxel size for the patients were 0.6 mm × 0.6 mm × 0.6 mm, 0.9 mm × 0.9 mm × 1.2 mm or 1 mm × 1 mm × 1 mm (see supplement for details). One day after surgical ECoG electrode array placement, a high resolution 3D CT scan was made to locate the electrodes (Philips Tomoscan SR7000, voxel size 0.5 mm × 0.5 mm × 1 mm).

First the CT was coregistered and re-sliced to the MRI coordinate frame, using a normalized mutual information routine in the SPM5 analysis environment (Fig. 1A–C) (Wells et al., 1996). Mutual information based coregistration has been developed to coregister images from multiple modalities and previous studies have shown that mutual information performs well for the coregistration of CT and MR images (Hill et al., 2001; Maes et al., 1997; Studholme et al., 1996; West et al., 1999) Approximate locations of desired
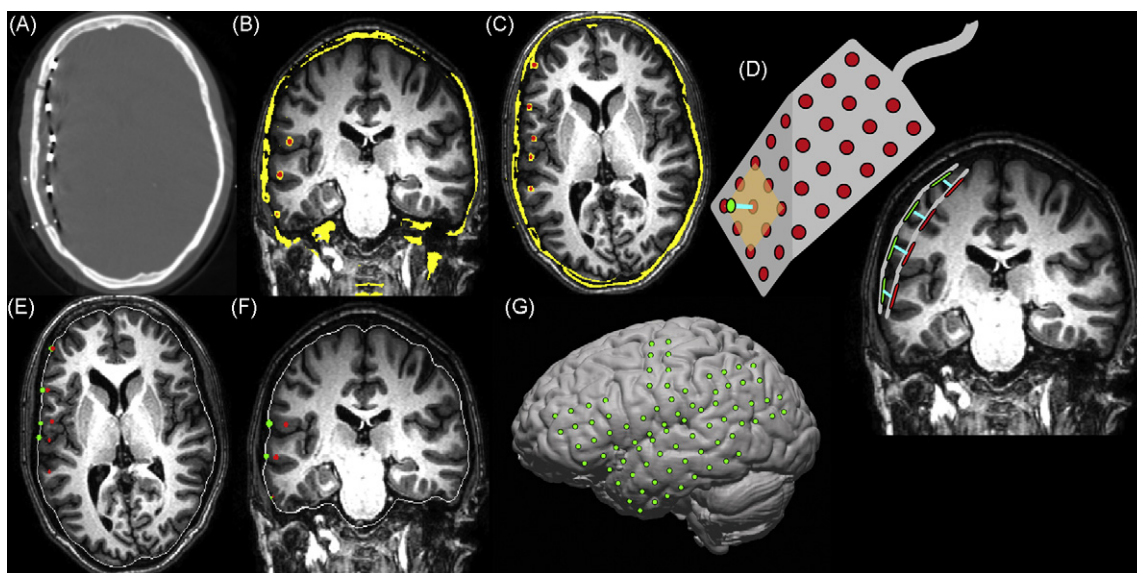

Fig. 1. Projection method. (A) One slice of the CT scan. (B and C) Thresholded CT (yellow) with detected electrodes (red) overlaid on an MRI, the brain shift, with electrodes shifted beneath the pre-implantation surface. (D) Schematic representation of the projection method. Electrodes are located under the cortical surface (red), are projected to the cortical surface in the direction of the norm of the grid (blue lines), resulting in locations on the cortical surface (green). (E and F) Example for patient 1, original electrode positions (red), cortical surface (white) and projected electrodes (green). (G) Rendering of the cortex with projected electrodes.

electrodes were identified manually on the CT by selecting high intensity clusters. Then these clusters were automatically masked by way of thresholding (watershed) and the center of mass of each cluster was assumed to be the location of an electrode. Each electrode was projected from the location found on the CT to the cortical surface of the coregistered MRI scan (Fig. 1D) using the following procedure: the MRI was segmented into grey and white matter compartments using unified segmentation in SPM5 (Ashburner and Friston, 2005). These compartments were combined into one image, and the resulting volume was then smoothed and thresholded (see supplemental material Table S1), yielding a smoothed cortical surface to which shifted electrodes could be automatically projected (Fig. 1E and F). Each electrode was then projected to the point on the surface in the direction of the local norm vector of the electrode grid (Fig. 1D). The local norm vector was the vector perpendicular to the plane defined by a principal component analysis of a matrix A, where matrix A contains the coordinates on the electrode and its nearest neighbors. For grids consisting of two rows, the electrode of interest and its three nearest neighbors were used to calculate the local norm vector. For grids consisting of single rows it is impossible to calculate a unique norm vector and these are projected to the closest point on the cortical surface.

2.3. Validation

To estimate the accuracy of the projection method, the projected electrodes were visualized on a 3D rendering of the cortical surface (Figs. 1D and 2C), and compared to photos taken during implantation (preoperative photo) and explantation (postoperative photo) of the electrodes for patients 1–6 (no postoperative photos were available for patient number six, and for this patient only the preoperative photo was used for verification of the projection). We used MATLAB and Adobe Photoshop (Adobe Systems, Inc., San Jose, CA, USA) to match the photo to the rendering with computed electrode locations. While on the rendering of the brain the sulci were clearly visible, on the operative photos only blood vessels were clearly visible as landmarks of cortical anatomy. Therefore a reference photo of the brain without electrodes (taken immediately before implantation, Fig. 2B) was used on which both blood vessels and sulci could be marked (Fig. 2D and E respectively). Sulci on the rendering of the brain with the projected electrodes were matched to sulci on the reference photo (Fig. 2F and H) and blood vessels on the pre- and postoperative photos were matched to blood vessels on the reference photo (Fig. 2A and G). Fig. 2F shows how affine and non-affine transformations were used to visually match these photos and that relative positions between sulci and electrode locations were preserved. With affine transformations (rotations, translations and resizing) the rendering and photo with electrodes were roughly matched to sulci and vasculature of the reference photo. After only affine transformations, mainly edges were not accurately registered to the reference photo as shown in the bottom panel in Fig. 2F. Warping (in Adobe Photoshop CS3) was subsequently applied only at the edges of the rendering or photo to accurately coregister these to the reference photo (blind to the electrode locations which were repositioned together with the warping). Supplementary Fig. S1 shows the matched photos for
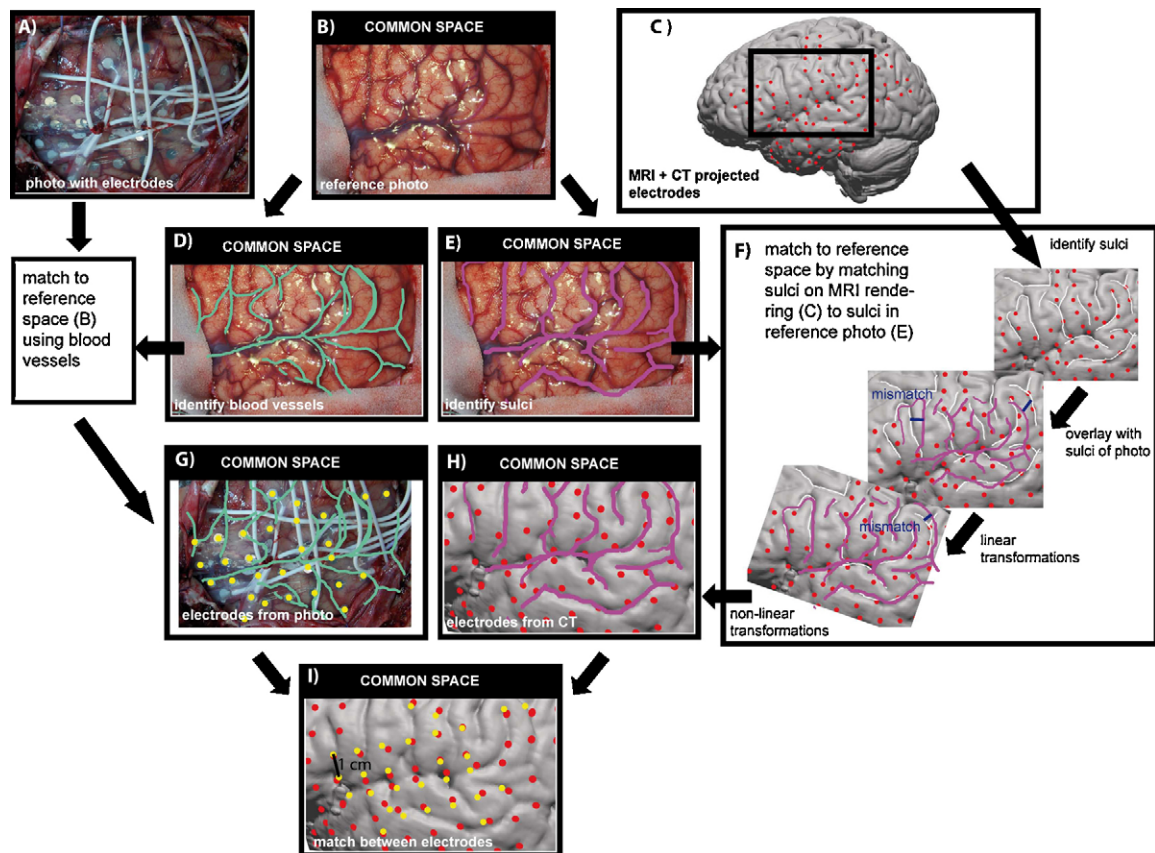
Fig. 2. Validation of the projection method. In a reference intra-operative photo (B) blood vessels (cyan, in D) and sulci (pink, in E) were marked. On the rendered surface (MRI) with projected electrodes (C) sulci were identified (white) and matched to the sulci on the photo (pink) (F). Both linear and non-linear transformations were required to obtain a good match between sulci. In blue the initial mismatch, and mismatch after linear transformation is marked. Note that these transformations do not affect relative positions between electrodes (red) and sulci (white) on the rendering. The same procedure was performed to match blood vessels on the reference photo (D) to blood vessels on the operative photo with electrodes (A). After registering all photos into common space, the rendering of the brain was visualized with projected electrodes (red) and electrodes from the operative photo (yellow) (H). Within a grid, spacing between electrodes was 1 cm.

all subjects. Electrodes on these matched pictures were overlaid and center-to-center distances between electrodes on operative photos and projected electrodes were calculated (Fig. 2I). On each picture a reference pair of adjacent electrodes (with a known center-to-center distance of 1 cm) was used to determine the scale.

2.4. Application example

To illustrate the usefulness of this method, fMRI with ECoG results of a motor task were overlaid in patient 7. In the motor task the patient moved the thumb during four (fMRI) or five (ECoG) 30 s blocks of movement (thumb flexion/extension at the rate of 2 Hz) alternated with five or six 30 s blocks of rest respectively.

Before surgery fMRI scans were acquired on a 3 T scanner with a 3D PRESTO scan (Neggers et al., 2008; Ramsey et al., 1998). In one run 340 volumes were acquired with the following parameters: TR/TE 22.5/32.4 ms, flip angle 10°, FOV = 256 mm × 224 mm × 160 mm, acquisition voxel size 4 mm isotropic. Using SPM5 functional images were realigned and coregistered with the anatomical image. A general linear model, including a regressor for motor activation (block design) and realignment parameters to control for movement artifacts, was estimated. The regression coefficient map for the motor task was converted to a statistical map with t-values for assessment of the regions involved in thumb movement, results are reported at $t > 3.11$ ($p < 0.001$, uncorrected).

The same task was performed by the patient during ECoG recordings. ECoG data were acquired with a 128 channel recording system (SD-128, Micromed, Treviso, Italy) with a sampling rate of 512 Hz, and were band-pass filtered (0.15–134.4 Hz). Signals were re-referenced to the common average of all intracranial electrodes and two second epochs were extracted from movement and rest blocks (respectively 70 and 85 epochs). For each of these epochs, the power spectral density was calculated every 1 Hz by Welch's method (Welch, 1967) with 250 ms windows, overlap of 125 ms and a Hamming window to attenuate edge effects. After normalizing (by element-wise division) the power spectra of each epoch with respect to the mean power over all epochs at each frequency, the log of the normalized power was averaged from 75 to 95 Hz. A t-test was performed on the average log normalized power for each electrode over movement versus rest epochs to assess which electrodes showed significant increases in power during movement. Results are reported at $p < 0.05$, Bonferroni corrected for multiple comparisons over electrodes.
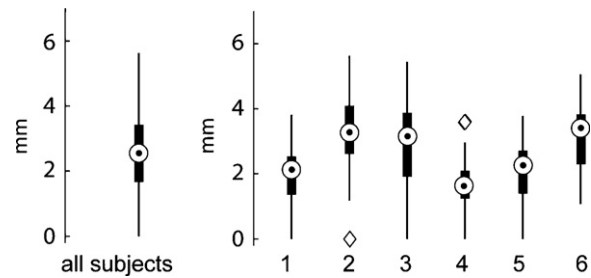
3. Results

3.1. Technique

Electrodes were projected to the surface of the brain in the direction orthogonal to the local surface of the shifted cortex (Fig. 1). Supplemental Fig. S2 shows for one subject that a lateral projection would have led to substantially different results. For each patient, the projection procedure, including up to 128 electrodes, took less than 2 h (including preprocessing of MR and CT scans, for any of three users).

3.2. Validation

Distances between electrodes on the photo and the projection are shown in Fig. 3 for patients 1–6 (postoperative photos for patients 1–5, preoperative for patient 6, supplemental Fig. S1). The median distance between the projected electrodes and electrodes

Fig. 3. Validation results. Box-plots of the distance between projected electrodes and electrodes on the operative photo with all subjects included and for each subject individually. Circles indicate the median distance, thick bars 50% of the distribution, thin bars indicate the maximum and minimum distance, outliers are indicated by diamonds (points larger than $q_3 + 1.5(q_3 - q_1)$ or smaller than $q_1 - 1.5(q_3 - q_1)$ with q_1 and q_3 the 25th and 75th percentile respectively).

on the photo was 2.6 mm (less than 3.4 mm for 75% of the electrodes, less than 5.6 mm for all electrodes). The same results were obtained when preoperative photos were used (median distance to preoperative photo = 2.4 mm, range 0–6.8 mm) and the distance of the projected electrodes to electrodes on the pre- and postoperative photo did not differ (nonparametric Wilcoxon rank sum test, $p = 0.92$).

3.3. Application example

Fig. 4A shows the craniotomy of patient 7 where only 19 out of 104 ECoG electrodes were visible. Electrodes that showed significant power differences ($p < 0.05$ Bonferroni corrected) in high frequencies (75–95 Hz) during thumb movement compared to rest were located outside the craniotomy on the pre- and postcentral gyri (Fig. 4B). All electrodes were located in or near areas that showed significant differences in BOLD activation ($t_{(325)} > 3.11$, $p < 0.001$ uncorrected) during the same motor task.

4. Discussion

The identification of the exact location of the electrodes is an important issue in ECoG research. This study first presents a method to localize ECoG electrodes on an individual, preoperative MRI scan. The MRI was coregistered with a CT scan made after implantation of the ECoG electrodes. The CT was then used to localize the ECoG electrodes and these electrodes were automatically projected on the cortical surface of the MRI. Second, to validate the method, a comparison between projected electrode locations and operative photos in six patients showed that this method localized electrodes to a 2.6 mm median accuracy, a value that is in the order of the electrode diameter (2.3 mm). Third, to illustrate the utility of the method we show a match between fMRI and ECoG data from a motor task for one patient with electrodes on the sensorimotor areas outside the craniotomy.

Electrodes were projected to the surface of the brain, correcting for a brain shift that can be on the order of 1 cm or more (Dalal et al., 2008; Hill et al., 2000). To enable an automatic procedure, it was assumed that electrodes have to be projected orthogonal to the local surface of the shifted cortex and that this transformation would be a good approximation of the brain shift. Other corrections for the brain shift, such as a simple lateral projection, would have led to substantially different results. An orthogonal projection is a simple transformation that proves to be robust and the validation with photos shows that its results are reliable across subjects. Similar precision to this study was reported by Dalal et al. (2008) who presented a semi-automated method in which X-rays and operative photos are used to visually localize electrodes on a preoperative MRI. Visually matching electrode positions are, however,
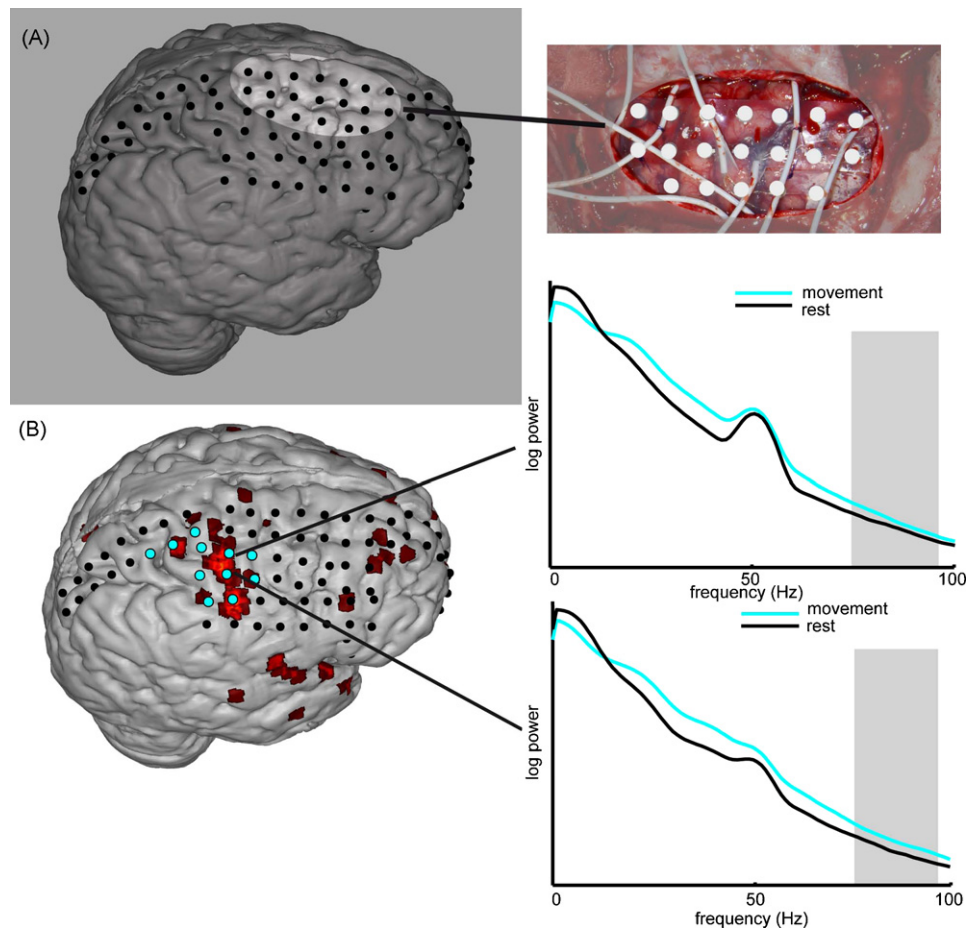
Fig. 4. Illustration of the technique in practice. (A) Craniotomy indicated on the rendering of the cortical surface with electrode positions and photo. (B) Rendering of the cortical surface with in red fMRI regions that were significantly activated by left thumb movement compared to rest ($t_{(325)} > 3.11$, $p < 0.001$ uncorrected). In cyan: electrodes with significant increases in power in the high frequency bands (75–95 Hz) during movement compared to rest ($p < 0.05$ Bonferroni corrected for total number of electrodes). For two electrodes that showed a significant difference, power spectra averaged over movement (cyan) and rest (black) epochs are shown. At 50 Hz a line noise (ambient contamination) peak is visible. (For interpretation of the references to colour in this figure legend, the reader is referred to the web version of the article.)

much more time consuming and depend heavily on the expertise of the experimenter. Our method is, with respect to matching procedure is independent of human expertise and most importantly, it does not rely on photos and therefore yields reliable results in electrodes positioned under the skull away from the opening.

A critical step in our study is the accuracy of the coregistration of CT and MRI scans. For coregistration of CT and MRI scans mutual information was applied, because many previous studies have shown that it yields very accurate matching results (Hill et al., 2001; Maes et al., 1997; Studholme et al., 1996; West et al., 1999), see also Pluim et al. (2003) for a survey of these studies. Although for the purpose of the present study a high resolution MRI scan was obtained for high detail of surface rendering, lower resolution MRI scans (which may be the standard in many clinical settings) can be expected to yield the same results in terms of accuracy of matching (see also West et al., 1999). The fact that mutual information based coregistration uses all voxels in the images and it does not assume a specific functional relationship between tissue intensities across modalities ensures a reliable global match between two images of different modalities (Roche et al., 2000).

The accuracy of the projection method was validated using photos of the brain taken during implantation and explantation of the grids. Operative photos can be used as a gold standard of electrode positions, but others have reported that there can be a difference in electrode positions between pre- and postoperative photos (Wellmer et al., 2002). Electrodes can be shifted during

closure of the dura after implantation as well as during opening before explantation. However, the distance between the projected electrodes and electrodes on pre- or postoperative photos did not differ.

To illustrate a potential benefit of the method, an example is shown where the relationship between fMRI and ECoG may be investigated even if electrodes are outside the craniotomy. In such cases, photographs would be of no use for invisible electrodes, limiting investigation to visible cortex. Given our estimate of projection accuracy based on the present study, and the reasonable assumption that the correction method yields equal results for visible and non-visible electrodes, the example illustrates an added value of the technique.

There are several other advantages in using this technique, one of which is that it is fully automated. It is readily implemented, since it only requires MATLAB and SPM5. As long as the surface of a volume can be estimated, electrodes can be projected in the direction of the norm vector of the grid to the closest point on the surface. When one hemisphere is removed from the MRI, interhemispheric electrodes can be localized and the same can be done for subtemporal electrodes after segmentation and removal of the cerebellum. Coregistration with other medical images such as angiograms is also possible, allowing one to see whether an electrode is located on a blood vessel. When projecting the electrodes to an individual MRI scan, the electrode coordinates are specific for the subjects' brain volume, and when normalizing this to MNI or Talairach space,

coordinates in these standard spaces can easily be extracted. Only a high resolution pre-implantation MRI and a high resolution post-implantation CT scan are required and the software is available upon request from the authors.

In conclusion, this method enables localization of ECoG electrodes on individually rendered cortical surfaces. It enables rapid and accurate localization of ECoG measures to brain anatomy. ECoG measures can now be seamlessly integrated with findings from other experimental modalities, such as fMRI, constituting a powerful tool for exploration of neural physiology in humans.

Acknowledgements

Appendix A. Supplementary data

Supplementary data associated with this article can be found, in the online version, at doi:10.1016/j.jneumeth.2009.10.005.

References

Ashburner J, Friston KJ. Unified segmentation. NeuroImage 2005;26:839–51.

Ball T, Schulze-Bonhage A, Aertsen A, Mehring C. Differential representation of arm movement direction in relation to cortical anatomy and function. J Neural Eng 2009;6:016006.

Bhavaraju NC, Nagaraddi V, Chetlapalli SR, Osorio I. Electrical and thermal behavior of non-ferrous noble metal electrodes exposed to MRI fields. Magn Reson Imaging 2002;20:351–7.

Canolty RT, Edwards E, Dalal SS, Soltani M, Nagarajan SS, Kirsch HE, et al. High gamma power is phase-locked to theta oscillations in human neocortex. Science 2006;313:1626–8.

Cooper R, Winter AL, Crow HJ, Walter WG. Comparison of subcortical, cortical and scalp activity using chronically indwelling electrodes in man. Electroencephalogr Clin Neurophysiol 1965;18:217–28.

Crone NE, Boatman D, Gordon B, Hao L. Induced electrocorticographic gamma activity during auditory perception. Brazier Award-winning article, 2001. Clin Neurophysiol 2001a;112:565–82.

Crone NE, Hao L, Hart Jr J, Boatman D, Lesser RP, Irizarry R, et al. Electrocorticographic gamma activity during word production in spoken and sign language. Neurology 2001b;57:2045–53.

Crone NE, Miglioretti DL, Gordon B, Lesser RP. Functional mapping of human sensorimotor cortex with electrocorticographic spectral analysis. II. Event-related synchronization in the gamma band. Brain 1998a;121:2301–15.

Crone NE, Miglioretti DL, Gordon B, Sieracki JM, Wilson MT, Uematsu S, et al. Functional mapping of human sensorimotor cortex with electrocorticographic spectral analysis. I. Alpha and beta event-related desynchronization. Brain 1998b;121:2271–99.

Dalal SS, Edwards E, Kirsch HE, Barbaro NM, Knight RT, Nagarajan SS. Localization of neurosurgically implanted electrodes via photograph-MRI-radiograph coregistration. J Neurosci Methods 2008;174:106–15.

Edwards E, Soltani M, Deouell LY, Berger MS, Knight RT. High gamma activity in response to deviant auditory stimuli recorded directly from human cortex. J Neurophysiol 2005;94:4269–80.

Hill DL, Batchelor PG, Holden M, Hawkes DJ. Medical image registration. Phys Med Biol 2001;46:R1–45.

Hill DL, Smith AD, Simmons A, Maurer Jr CR, Cox TC, Elwes R, et al. Sources of error in comparing functional magnetic resonance imaging and invasive electrophysiological recordings. J Neurosurg 2000;93:214–23.

Maes F, Collignon A, Vandermeulen D, Marchal G, Suetens P. Multimodality image registration by maximization of mutual information. IEEE Trans Med Imaging 1997;16:187–98.

Miller KJ, Leuthardt EC, Schalk G, Rao RP, Anderson NR, Moran DW, et al. Spectral changes in cortical surface potentials during motor movement. J Neurosci 2007a;27:2424–32.

Miller KJ, Makeig S, Hebb AO, Rao RP, denNijs M, Ojemann JG. Cortical electrode localization from X-rays and simple mapping for electrocorticographic research: the "Location on Cortex" (LOC) package for MATLAB. J Neurosci Methods 2007b;162:303–8.

Miller KJ, Zanos S, Fetz EE, den Nijs M, Ojemann JG. Decoupling the cortical power spectrum reveals real-time representation of individual finger movements in humans. J Neurosci 2009;29:3132–7.

Neggers SF, Hermans EJ, Ramsey NF. Enhanced sensitivity with fast three-dimensional blood-oxygen-level-dependent functional MRI: comparison of SENSE-PRESTO and 2D-EPI at 3 T. NMR Biomed 2008;21:663–76.

Nir Y, Mukamel R, Dinstein I, Privman E, Harel M, Fisch L, et al. Interhemispheric correlations of slow spontaneous neuronal fluctuations revealed in human sensory cortex. Nat Neurosci 2008;11:1100–8.

Noordmans HJ, van Rijen PC, van Veelen CW, Viergever MA, Hoekema R. Localization of implanted EEG electrodes in a virtual-reality environment. Comput Aided Surg 2001;6:241–58.

Pfurtscheller G, Graimann B, Huggins JE, Levine SP, Schuh LA. Spatiotemporal patterns of beta desynchronization and gamma synchronization in corticographic data during self-paced movement. Clin Neurophysiol 2003;114:1226–36.

Pluim JP, Maintz JB, Viergever MA. Mutual-information-based registration of medical images: a survey. IEEE Trans Med Imaging 2003;22:986–1004.

Ramsey NF, van den Brink JS, van Muiswinkel AM, Folkers PJ, Moonen CT, Jansma JM, et al. Phase navigator correction in 3D fMRI improves detection of brain activation: quantitative assessment with a graded motor activation procedure. NeuroImage 1998;8:240–8.

Roche A, Malandain G, Udupa JK. Unifying maximum likelihood approaches in medical image registration. Int J Imaging Syst Technol 2000;11:71–80.

Schulze-Bonhage AH, Huppertz HJ, Comeau RM, Honegger JB, Spreer JM, Zentner JK. Visualization of subdural strip and grid electrodes using curvilinear reformatting of 3D MR imaging data sets. AJNR Am J Neuroradiol 2002;23:400–3.

Sinai A, Bowers CW, Crainiceanu CM, Boatman D, Gordon B, Lesser RP, et al. Electrocorticographic high gamma activity versus electrical cortical stimulation mapping of naming. Brain 2005;128:1556.

Studholme C, Hill DL, Hawkes DJ. Automated 3-D registration of MR and CT images of the head. Med Image Anal 1996;1:163–75.

Studholme C, Novotny E, Zubal IG, Duncan JS. Estimating tissue deformation between functional images induced by intracranial electrode implantation using anatomical MRI. NeuroImage 2001;13:561–76.

Welch P. The use of fast Fourier transform for the estimation of power spectra: a method based on time averaging over short, modified periodograms. IEEE Trans Audio Electroacoustics 1967;15:70–3.

Wellmer J, von Oertzen J, Schaller C, Urbach H, Konig R, Widman G, et al. Digital photography and 3D MRI-based multimodal imaging for individualized planning of resective neocortical epilepsy surgery. Epilepsia 2002;43:1543–50.

Wells III WM, Viola P, Atsumi H, Nakajima S, Kikinis R. Multi-modal volume registration by maximization of mutual information. Med Image Anal 1996;1:35–51.

West J, Fitzpatrick JM, Wang MY, Dawant BM, Maurer Jr CR, Kessler RM, et al. Retrospective intermodality registration techniques for images of the head: surface-based versus volume-based. IEEE Trans Med Imaging 1999;18:144–50.

Yoshor D, Bosking WH, Ghose GM, Maunsell JH. Receptive fields in human visual cortex mapped with surface electrodes. Cereb Cortex 2007;17:2293–302.